

Heat Flow through Nonideal Contacts in Hot-Carrier Solar Cells

Abhinav S. Sharma[✉], Muhammad Hanif, Stephen P. Bremner, Michael P. Nielsen, Murad J. Y. Tayebjee, Fiacre E. Rougieux, Nicholas J. Ekins-Daukes, and Andreas Pusch

School of Photovoltaic and Renewable Energy Engineering, UNSW Sydney, Kensington 2052, Australia

(Received 29 March 2023; revised 5 July 2023; accepted 26 July 2023; published 1 September 2023)

Hot-carrier solar cells (HCSCs) are optoelectronic heat engines that could, in principle, achieve efficient solar energy conversion with a high detailed-balance limit of 85% at full solar concentration. Approaching this limit requires negligible carrier energy loss to the lattice and reversible carrier extraction via narrow, highly conductive energy windows. Practical implementations of HCSCs with nonideal contacts such as two-dimensional (2D) contacts and thermionic barriers have excess heat flows resulting in irreversible extraction. We examine the electronic heat flows in such schemes to explain where power losses originate and show that they determine carrier temperatures and device performance, providing insight into optimal characteristics of an HCSC. A compromise between maximizing current extraction and minimizing the associated heat flow determines the optimal extraction energy. This optimization for a thermionic barrier contact shows that remarkably low carrier temperatures (~ 500 K) are required for optimal operation at 45% efficiency for a 1-eV-band-gap absorber under the particle conservation model, compared to ~ 1000 K at 60% efficiency for a black-body absorber under the impact ionization model, even in the absence of carrier-phonon interactions. Furthermore, we quantify the irreversible component of the heat flow and show that it is minimal for highly conductive 2D contacts that approach the Carnot limit. The results suggest that heat flows in HCSCs can be probed by measuring carrier temperature trends by varying applied bias and contact parameters, which may present clearer evidence of HCSC operation.

DOI: 10.1103/PhysRevApplied.20.034001

I. INTRODUCTION

Hot-carrier solar cells (HCSCs) present an attractive way of reaching high efficiencies in solar energy conversion. Using a single absorber material and energy-selective contacts (ESCs), 85% efficient conversion can be achieved under full solar concentration [1,2]. This is possible because the fundamental loss of the excess kinetic energy of the photoexcited carriers to the lattice is recovered [3]. However, that efficiency limit is based on several idealizations. Firstly, the carriers in the absorber are required to efficiently equilibrate among themselves to form a thermal distribution, but carrier cooling via the lattice should be slow such that the distribution is maintained at a temperature higher than the lattice [4]. Secondly, carrier extraction through ESCs must be reversible such that the HCSC operates as an isentropic Carnot engine. This is achieved when the energy range of extraction is infinitesimal and contact conductivity simultaneously goes to infinity to eliminate resistance losses.

The single-junction detailed-balance limit is calculated by considering particle conservation of photons and charge carriers. Particle conservation neglects processes such as

Auger recombination (and its reverse process, impact ionization), as these do not conserve particle number. Energy conservation is not considered for conventional single-junction devices since the excess kinetic energy of carriers is lost to the lattice. On the other hand, since HCSCs utilize the excess kinetic energy of carriers, energy conservation also needs to be considered. Ross and Nozik [1] calculated the efficiency limit by considering both energy and particle conservation (henceforth referred to as the “particle conservation model”). However, calculations using this approach have been shown to result in mathematical contradictions in short-circuit conditions [5]. Furthermore, for low band gaps, Auger processes become significant, making the particle conservation assumption invalid [5,6]. Assuming the rates of impact ionization and Auger recombination dominate to the extent that no quasi-Fermi-level separation (QFLS) can be maintained in the absorber, Würfel [2] calculates the efficiency limit for a black-body absorber, arriving at the same efficiency limit as Ross and Nozik [1] under full concentration. We refer to this model as the “impact ionization model.” The efficiency limits are obtained under the assumption of no energy loss via phonons (no carrier cooling). The particle conservation and impact ionization models are limiting cases of extremely inefficient and efficient impact-Auger processes, respectively.

* abhinav.sharma@unsw.edu.au

No systems have been found to approach these idealized limits, but, while an efficient HCSC has not been demonstrated, proofs of concept do exist [7–10]. Maintaining sufficiently high carrier temperatures requires absorber materials with appropriate electron-phonon and phonon-phonon interactions, since the main excess energy-loss channel for carriers is typically via phonons to the lattice where it is dissipated as waste heat. Wide ranges of materials and material systems are being explored that may allow slow carrier cooling [11–17]. ESCs are usually implemented via resonant tunneling structures using quantum dots (QDs) or quantum wells [10,18] or thermionic barrier structures [8,9,19]. Low-dimensional contacts such as QDs are energy-selective but with a finite width of energies through which electrons can be transmitted [20,21]. The thermionic barrier, on the other hand, is a semi-infinite filter, and it is momentum-selective rather than energy-selective. It has been shown that momentum selectivity allows fewer electrons to contribute to the current than energy selectivity [20].

All practical devices will have losses additional to the ideal thermodynamic limit. Theoretical explorations have shown that a nonideal absorber with a finite electron-lattice thermalization time results in lower carrier temperatures and efficiencies [4,22,23]. Nonideal contacts result in irreversible carrier extraction, resulting in entropy production and a reduced efficiency [24–26].

In this work we investigate the effects of these nonideal contacts and how optimal contact configurations relate to the heat flows associated with carrier extraction. First, we introduce the thermodynamics of HCSCs in Sec. II, followed by describing the detailed-balance model in Sec. III. We explore the application of detailed balance for the impact ionization and particle conservation models in Secs. IV and V, respectively. We compare and contrast these models and summarize our findings in Sec. VI.

II. THE HCSC AS A HEAT ENGINE

To understand the heat flows associated with HCSC operation, we consider the HCSC as an electronic heat engine, illustrated in Fig. 1. The hot side of the electronic heat engine is the absorber at temperature T_H . It is not a reservoir since it is heated at a finite rate by the Sun, modeled with a temperature T_{Sun} . Consequently, T_H will depend on the operating conditions. The cold side of the engine is the contact, which is assumed to be efficiently coupled with a reservoir at T_C that fixes its temperature.

For the heat engine, we consider energy balance,

$$P = \dot{Q}_H - \dot{Q}_C, \quad (1)$$

where the power output P of the engine is the difference between the incoming heat flow \dot{Q}_H from the hot reservoir and the heat flow \dot{Q}_C dissipated to the cold reservoir. The

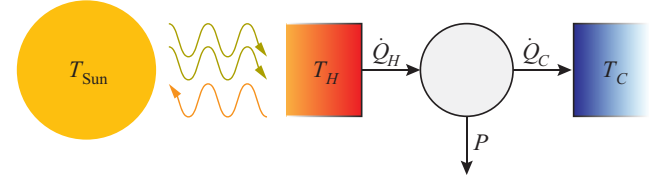


FIG. 1. An HCSC extracts power P from excess carrier kinetic energy by operating as a heat engine between carriers at temperature T_H in the absorber which are heated by the Sun (at temperature T_{Sun}) and cold carriers at temperature T_C in the contact. The portion of the total heat flow from the absorber (associated with electronic flow) \dot{Q}_H not converted to power is dissipated as excess heat flow \dot{Q}_C to the contacts.

net entropy flux is

$$\dot{S} = \frac{\dot{Q}_C}{T_C} - \frac{\dot{Q}_H}{T_H}, \quad (2)$$

where T_H and T_C are the electron temperatures in the hot and cold reservoirs, respectively.

By the second law of thermodynamics, $\dot{S} \geq 0$. In a reversible (Carnot) engine, $\dot{S} = 0$, minimizing the excess heat flow \dot{Q}_C that is lost to the cold reservoir for a given P . The power is then given by

$$P = \eta_{\text{Carnot}} \dot{Q}_H, \quad (3)$$

where $\eta_{\text{Carnot}} = 1 - (T_C/T_H)$ is the Carnot efficiency. Therefore, for an ideal HCSC with fully reversible ESCs, for a given output power, we have the minimal dissipated heat flow

$$\dot{Q}_C = \dot{Q}_{\text{rev}} = \frac{P}{\eta_{\text{Carnot}}} - P = P \left(\frac{1}{1 - (T_C/T_H)} - 1 \right),$$

giving

$$\dot{Q}_{\text{rev}} = P \left(\frac{T_C}{T_H - T_C} \right). \quad (4)$$

The heat flow in the nonideal case can therefore be separated into the thermodynamically required reversible component (\dot{Q}_{rev}) and the excess nonideal loss (\dot{Q}_{irrev}), i.e., $\dot{Q}_C = \dot{Q}_{\text{rev}} + \dot{Q}_{\text{irrev}}$. Therefore, we can calculate the excess heat flow as

$$\dot{Q}_{\text{irrev}} = \dot{Q}_C - P \left(\frac{T_C}{T_H - T_C} \right). \quad (5)$$

Because \dot{Q}_{irrev} leads to entropy production in the electronic heat engine, it can be related to the change in entropy using

Eqs. (1), (2), and (5), giving

$$\dot{Q}_{\text{irrev}} = \dot{S} \left(\frac{1}{T_C} - \frac{1}{T_H} \right). \quad (6)$$

Therefore, \dot{Q}_{irrev} is a measure of the irreversibility of the heat engine.

In addition to operating as a heat engine, an HCSC can harness energy via $\Delta\mu$, the QFLS in the absorber [26]. In the case of ideal energy-selective contacts, the voltage V is given by [27]

$$V = \frac{1}{q} \left(\eta_{\text{Carnot}} E_c + \Delta\mu \frac{T_C}{T_H} \right), \quad (7)$$

where E_c is the contact energy. Equation (3) therefore no longer holds; instead, we have

$$P = \left(\eta_{\text{Carnot}} + \frac{\Delta\mu}{E_c} \frac{T_C}{T_H} \right) \dot{Q}_H. \quad (8)$$

When assessing HCSCs with nonideal contacts, the heat flow is not associated with a single energy E_c . To evaluate \dot{Q}_{irrev} , we replace E_c with the average energy of the transmitted carriers E_{avg} . Then \dot{Q}_{irrev} is given by

$$\dot{Q}_{\text{irrev}} = \dot{Q}_C - P \left(\frac{1}{\left(\eta_{\text{Carnot}} + \frac{\Delta\mu}{E_{\text{avg}}} \frac{T_C}{T_H} \right)} - 1 \right). \quad (9)$$

Note that setting $\Delta\mu = 0$ gives the same expression as Eq. (5).

We use \dot{Q}_{irrev} as a measure of the irreversibility of an HCSC contact, and show its role in contact optimization.

III. DETAILED BALANCE

We employ a detailed-balance model to evaluate the steady-state operating characteristics of HCSCs with nonideal contacts. The absorbed radiation is partially converted to electrical power, while the remainder is lost as radiation or as excess heat flow via carrier extraction. Assuming that the contact area is equal to the area of the illuminated absorber, the energy balance can be written as

$$0 = G_{\text{Sun}} + G_{\text{amb}} - R_{\text{rad}} - \dot{E}_{J,\text{out}} + \dot{E}_{J,\text{in}}, \quad (10)$$

where G_{Sun} and G_{amb} represent the power of the absorbed radiation from the Sun and the ambient, respectively, R_{rad} is the power of the radiation emitted by the hot-carrier absorber, and $\dot{E}_{J,\text{out}}$ and $\dot{E}_{J,\text{in}}$ are the energy flows associated with the current across the contacts. Some of the energy that flows into the contacts is converted to electrical power, given by $P_{\text{elec}} = IV$, where $I = I_{\text{out}} - I_{\text{in}}$ is the

net current and V is the voltage across the device, with the rest dissipated as heat.

In the impact ionization model for HCSCs, only energy balance is considered. For the particle conservation model, we additionally have

$$0 = \phi_{\text{Sun}} + \phi_{\text{amb}} - \phi_{\text{rad}} - \frac{J_{\text{out}}}{q} + \frac{J_{\text{in}}}{q}. \quad (11)$$

Here ϕ_{Sun} , ϕ_{amb} , and ϕ_{rad} are the absorbed and emitted photon fluxes associated with the Sun, the ambient, and radiative recombination in the absorber, respectively. The last two terms in Eq. (11) signify the carrier fluxes across the contacts.

We explore both of these models under nonideal contacting schemes, and study and compare their characteristics. The models are for an idealized absorber, hence the effects of electron-phonon interactions and defect- and/or trap-assisted recombination are not considered.

IV. IMPACT IONIZATION MODEL

Since the impact ionization model is not applicable for large band gaps, we consider a zero-band-gap black-body absorber for simplicity, which in practice could correspond to a metallic absorber [9]. The energy flux density absorbed from the Sun is then given by

$$G_{\text{Sun}} = f \sigma T_{\text{Sun}}^4, \quad (12)$$

with f the concentration factor ($f = 1$ for full concentration and $f = 1/46200$ for 1 Sun), σ the Stefan-Boltzmann constant, and T_{Sun} the temperature of the Sun, assumed to be 5800 K. For $f < 1$, the cell also receives radiation from the ambient (at temperature $T_C = 300$ K), given by

$$G_{\text{amb}} = (1 - f) \sigma T_C^4. \quad (13)$$

The radiation emitted by the black-body absorber is

$$R_{\text{rad}} = \sigma T_H^4, \quad (14)$$

where T_H is the temperature of the electrons in the absorber. This assumes that the steady-state carrier population is in quasiequilibrium and can hence be characterized by a temperature.

Current extraction and the associated energy flow depend on the contact configuration. The absorber-contact interface determines the contact conductivity and the transmission function $\xi(E)$. The transmission function selects a subset of electronic states that are capable of transmitting carriers through the contacts. We now consider these transmission functions and calculate the energy flows for QDs and thermionic barrier contacts, on the basis of which we then optimize the contact configurations.

A. Quantum dots

Quantum dots can be used for energy-selective carrier extraction by fabrication of double-barrier resonant tunneling structures [18]. Carrier extraction through such contacts depends on the energy E of the carriers, and is typically modeled with a Gaussian transmission function $\xi_{\text{Gaussian}}(E)$ centered around E_{ext} with width W_{ext} , given by

$$\xi_{\text{Gaussian}}(E) = \exp\left(-\frac{(E - E_{\text{ext}})^2}{2W_{\text{ext}}^2}\right). \quad (15)$$

Fundamentally, the electron energy transmission width is related to the lifetime of the state by the uncertainty relation, which in turn depends on parameters such as the thickness of the barrier layers [28]. However, W_{ext} is largely determined by broadening of energy levels of QDs associated with QD size inhomogeneities, and is of order 10 meV in practical QD systems [29,30]. Under the Landauer formalism, the current density through such low-dimensional contacts is given by [21]

$$J = \frac{2Nq}{h} \int_0^\infty [f_H(E) - f_C(E)] \xi_{\text{Gaussian}}(E) dE, \quad (16)$$

where N is the QD density, and f_C and f_H are the contact and absorber electron occupancies (under the Boltzmann approximation), respectively.

However, this does not consider an energy-dependent density of states and an effective mass at the interface. An alternative formalism that includes those factors is [20]

$$J = \frac{4\pi q m_{\text{eff}}}{h^3} \int_0^\infty E [f_H(E) - f_C(E)] \xi_{\text{Gaussian}}(E) dE. \quad (17)$$

For narrow windows, the two approaches yield similar results. In this case, an equivalence can be made between N and m_{eff} . Equating the coefficients gives

$$N = \frac{2\pi E_{\text{ext}} m_{\text{eff}}}{h^2}. \quad (18)$$

We study two-dimensional contacts using Eq. (16), and use Eq. (18) to deduce the corresponding effective mass in a three-dimensional system.

B. Thermionic barrier

For a semi-infinite thermionic barrier, we consider a step transmission function, given by

$$\xi_{\text{step}}(E) = \begin{cases} 0 & \text{if } E_z < E_{\text{ext}}, \\ 1 & \text{if } E_z \geq E_{\text{ext}}, \end{cases} \quad (19)$$

where $E_z = \hbar^2 k_z^2 / (2m_{\text{eff}})$ is the component of the kinetic energy of the carriers with momentum k_z towards the

contact, showing that the thermionic barrier is momentum-selective rather than energy-selective.

Making the Boltzmann approximation for the electron occupation functions, assuming a parabolic density of states, and a step transmission function, the Richardson-Dushman equation for the current can be derived [24], with the associated energy flux density given by

$$\dot{E}_{J,\text{out}} = 2 \exp\left(-\frac{E_{\text{ext}}}{kT_H}\right) 2\pi m_{\text{eff}} \left(\frac{k_B T_H}{h}\right)^3 \left(\frac{E_{\text{ext}}}{\frac{1}{2}k_B T_H} + 4\right), \quad (20)$$

where E_{ext} is the extraction energy and m_{eff} is the effective mass. The factor of 2 is to account for both the electron and hole contacts under the simplifying assumption of electron-hole symmetry. The mass m_{eff} is an interface property, but it generally can be assumed to be the lower of the absorber and contact effective masses [31]. Typical Richardson constants in heterostructures correspond to effective masses of 0.00005–0.5 [32–36]. To consider an upper limit, we set $m_{\text{eff}} = 1$ for the thermionic barrier simulations.

The backflow of cold carriers from the contact additionally depends on the Fermi level at the contact. Relative to the midpoint of the electron and hole bands (as per the convention shown in Fig. 2), the Fermi level at the contact is equal to $qV_C = qV/2$, giving

$$\dot{E}_{J,\text{in}} = 2 \exp\left(-\frac{E_{\text{ext}} - qV_C}{kT_C}\right) 2\pi m_{\text{eff}} \times \left(\frac{k_B T_C}{h}\right)^3 \left(\frac{E_{\text{ext}}}{\frac{1}{2}k_B T_C} + 4\right). \quad (21)$$

The potential difference between the contacts, and thus the voltage across the device, is $V = 2V_C$.

C. Results

Employing the impact ionization model, we have optimized QD contacts with a Gaussian transmission window [Eq. (16)] in an HCSC with a thermalization-free absorber. The conductivity, determined by the contact density N , and the width of the Gaussian window W_{ext} determine how closely the device approaches a Carnot engine [37]. For efficient extraction, the density of conduction channels would ideally be high and comparable to that of a degenerate semiconductor or a metal, which is $10^8 \text{ cm}^{-2} > N > 10^{12} \text{ cm}^{-2}$, and from Eq. (18) it is equivalent to $10^{-2} m_e > m_{\text{eff}} > 10^{-6} m_e$. The window width W_{ext} and height E_{ext} that give maximal efficiency depend on N .

By optimization of W_{ext} and E_{ext} for various N , it is observed that the higher conductivity achieved by a larger N allows for narrower window widths, as shown

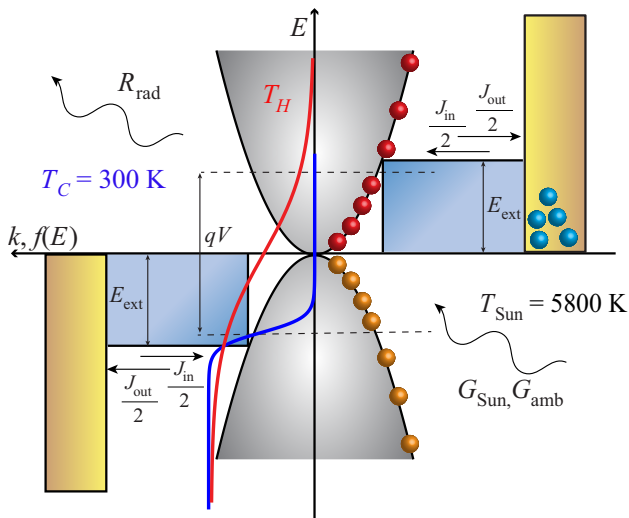


FIG. 2. Illustration of the detailed-balance HCSC model with thermionic barrier contacts, and its associated flows, assuming symmetric parabolic dispersion for electrons and holes. Generation from the Sun G_{Sun} (and the ambient G_{amb}) leads to hot electrons (red) and hot holes (orange), which recombine and radiate at temperature T_H . The carriers flow in (J_{in}) and out (J_{out}) of the absorber over barriers of height E_{ext} . The contacts are at ambient temperature T_C , with cold electrons (blue). The left side shows the hot and cold electron distribution functions. The properties of these distributions determine the operating point of the device.

in Fig. 3(a). This is because a high current can be maintained while minimizing excess heat flow. This results in a decreased irreversible fraction of the extraction heat flow $F_{\text{irrev}} = \dot{Q}_{\text{irrev}}/G_{\text{Sun}}$, giving high efficiencies, as shown in Fig. 3(b). Beyond contact densities of 10^9 cm^{-2} (corresponding to windows with width of order 10^{-2} eV and below), the efficiencies asymptotically approach the Carnot limit. The \dot{Q}_{irrev} value obtained using the power output and the temperatures of the system [Eq. (5)] is therefore a measure of the nonideality of an HCSC contact. Note that attaining high efficiencies and approaching reversible extraction requires a simultaneous increase in N and decrease in W_{ext} .

In practice, devices such as QD-based infrared photodetectors have been fabricated with high dot densities, on the order of 10^{10} to 10^{11} cm^{-2} [38–41]. However, achieving a high percentage of electronically active QDs may be a challenge [42]. Fabrication challenges with low-dimensional contacts may mean that thermionic barrier devices are an easier route for HCSC demonstrations.

We now study the optimization of the thermionic barrier height, for which it is instructive to resolve the constituent energy flows at the maximum power point (MPP). Figure 4 shows energy flows and carrier temperatures for varying barrier heights under 1000 Suns illumination. In the absence of carrier-phonon interaction, the only channels

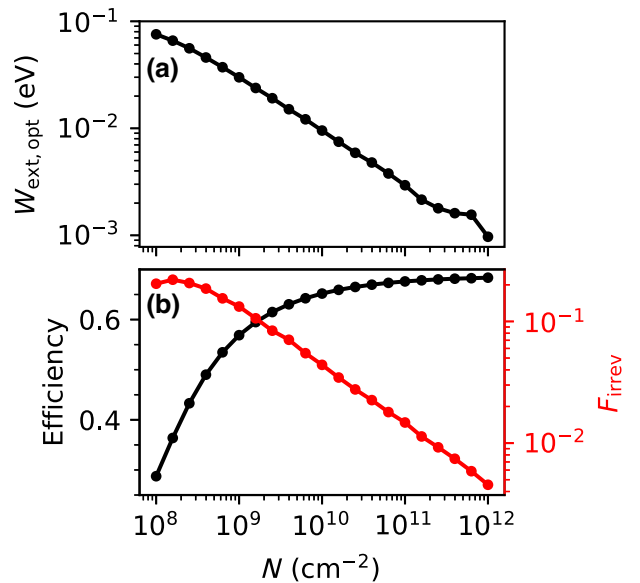


FIG. 3. Impact of contact conductivity on an HCSC with Gaussian window contacts under the impact ionization model operating under 1000 Suns. For a given N , the extraction energy E_{ext} and width W_{ext} of the contact were numerically optimized to maximize the efficiency. Shown are the optimal window width $W_{\text{ext},\text{opt}}$ (a), and the resulting efficiency [(b), black], as a function of contact density. The efficiency saturates as the contact approaches an ideal ESC, corresponding to a smaller irreversible fraction F_{irrev} [(b), red] of the extraction heat loss.

of energy loss are via carrier extraction and radiative recombination. The excess heat flow to the contacts resulting from carrier extraction is divided into its reversible and irreversible components using Eq. (5). Higher barrier heights result in minimal carrier extraction and hence a small excess heat flow to the contacts. While the contact is more reversible with a low \dot{Q}_{irrev} , the decreased current reduces the output power. While the electron temperature is high, most of the energy is lost via radiation. Lower barrier heights result in high electrical current, corresponding to a high heat flow to the contacts. This reduces the temperature of the electrons in the absorber. While the current drawn is large, the voltage drops and results in a low efficiency. Thus an optimal barrier of 1.6 eV results from a compromise between these effects, as also shown in Fig. 4 for $1000\times$ solar concentration. In the case of the ideal ESC, this compromise does not exist because changing the extraction energy leaves the product between current and voltage, and hence the electrical power, unchanged [27]. The dissipated heat flow is fixed to the minimal flow \dot{Q}_{rev} required from the second law for the given ratio of contact and absorber temperatures.

The temperature-voltage characteristics with the optimal barrier height are shown in Fig. 5. There is no significant change in temperature until the voltage is large enough to drive a significant back-current from the contacts into

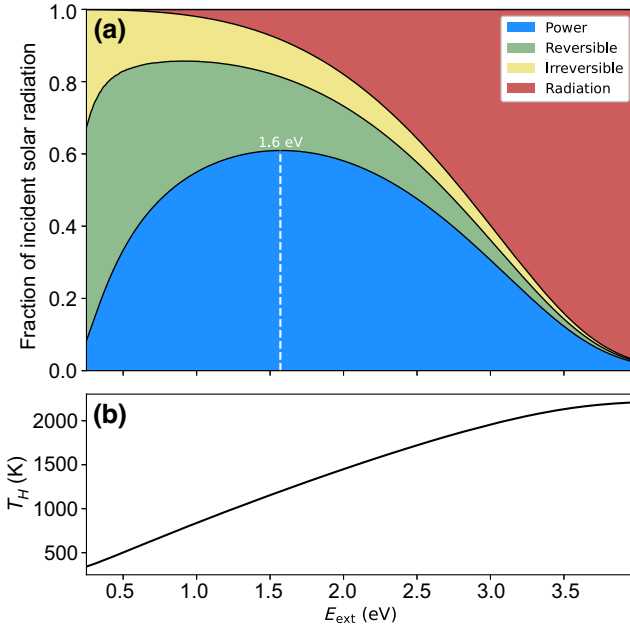


FIG. 4. (a) Breakdown of energy flows and (b) corresponding temperatures as a fraction of incident radiation (1000 Suns) in a thermionic barrier HCSC using the impact ionization model. The flows are shown for various barrier heights, showing how an optimal barrier results from a compromise between the conduction and radiation loss mechanisms. Note that the *x* axis is barrier height, *not* band gap as is common for single-threshold devices.

the absorber. At the open-circuit voltage (V_{oc}), this bias-induced back-current equals the outgoing current and no net electrical current flows. As this point is approached, the carrier temperature increases and an increasing proportion of the carrier energy is lost via radiation.

V. PARTICLE CONSERVATION MODEL

Semiconductor HCSCs can draw power from both the temperature differential and the electrochemical potential difference in the absorber manifested as a QFLS $\Delta\mu$ between conduction and valence bands. To introduce a QFLS, we additionally impose particle conservation as shown in Eq. (11).

A band gap E_g requires consideration of only a portion of the spectrum for generation and recombination. For a semiconductor with band gap E_g , by making the Boltzmann approximation for the spectral flux density of the radiation, the following general functional form for the energy flow is obtained:

$$\dot{E}(T, \Delta\mu, E_g, f) = \frac{2f\pi}{c^2 h^3} \exp\left(-\frac{E_g - \Delta\mu}{k_B T}\right) k_B T (6k_B T^3 + 6E_g k_B T^2 + 3E_g^2 k_B T + E_g^3). \quad (22)$$

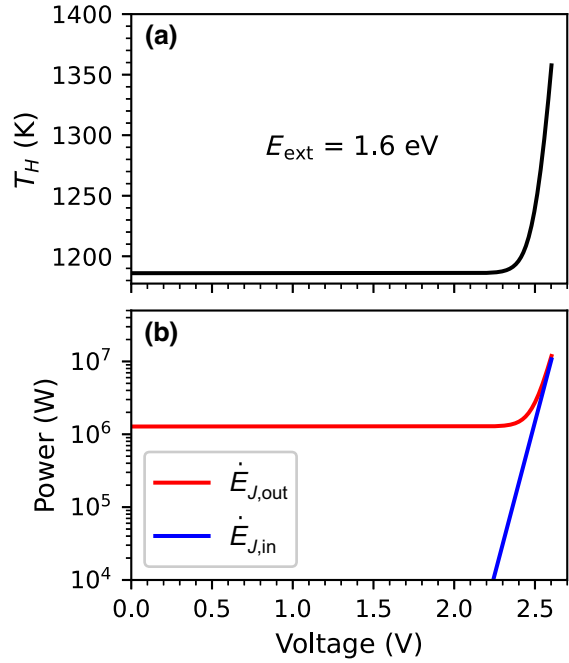


FIG. 5. Temperature-voltage characteristics of a thermionic barrier HCSC under the impact ionization model, operating under 1000 Suns with barrier height set to 1.6 eV. The carrier temperature is largely unchanged until the bias across the contacts is large enough to induce a significant back-current into the absorber, as shown in panel (b).

Particle conservation also requires consideration of the photon flux density, the general form of which is

$$\phi(T, \Delta\mu, E_g, f) = \frac{2f\pi}{c^2 h^3} \exp\left(-\frac{E_g - \Delta\mu}{k_B T}\right) k_B T (2k_B T^2 + 2E_g k_B T + E_g^2). \quad (23)$$

The energy flux density absorbed from the Sun is then given by

$$G_{\text{Sun}} = \dot{E}(T_{\text{Sun}}, 0, E_g, f_{\text{Sun}}), \quad (24)$$

and the absorbed photon flux density by

$$\phi_{\text{Sun}} = \phi(T_{\text{Sun}}, 0, E_g, f_{\text{Sun}}). \quad (25)$$

Similarly, the absorbed power and flux densities from the ambient are given by

$$G_{\text{amb}} = \dot{E}(T_0, 0, E_g, 1 - f_{\text{Sun}}) \quad (26)$$

and

$$\phi_{\text{amb}} = \phi(T_0, 0, E_g, 1 - f_{\text{Sun}}). \quad (27)$$

The emitted radiation power density by the electrons in the absorber is given by

$$R_{\text{rad}} = \dot{E}(T_H, \Delta\mu, E_g, 1) \quad (28)$$

and the photon flux density by

$$\phi_{\text{rad}} = \phi(T_H, \Delta\mu, E_g, 1). \quad (29)$$

Current extraction at a given contact under the particle conservation model additionally depends on the quasi-Fermi level, $\mu = \Delta\mu/2$. For a thermionic barrier, this gives

$$\dot{E}_{J,\text{out}} = 4\pi m_{\text{eff}} \left(\frac{k_B T_H}{h} \right)^3 \exp \left(-\frac{E_{\text{ext}} + \frac{1}{2}E_g - \mu}{kT_H} \right) \times \left(\frac{E_{\text{ext}} + \frac{1}{2}E_g}{\frac{1}{2}k_B T_H} + 4 \right), \quad (30)$$

$$J_{\text{out}} = \frac{4q\pi k_B^2 m_{\text{eff}} T_H^2}{h^3} \exp \left(-\frac{E_{\text{ext}} + \frac{1}{2}E_g - \mu}{kT_H} \right), \quad (31)$$

$$\dot{E}_{J,\text{in}} = 4\pi m_{\text{eff}} \left(\frac{k_B T_C}{h} \right)^3 \exp \left(-\frac{E_{\text{ext}} + \frac{1}{2}E_g - qV_C}{kT_C} \right) \times \left(\frac{E_{\text{ext}} + \frac{1}{2}E_g}{\frac{1}{2}k_B T_C} + 4 \right), \quad (32)$$

and

$$J_{\text{in}} = \frac{4q\pi k_B^2 m_{\text{eff}} T_C^2}{h^3} \exp \left(-\frac{E_{\text{ext}} + \frac{1}{2}E_g - qV_C}{kT_C} \right). \quad (33)$$

Because of convergence issues in the numerical simulations, we do not consider low-dimensional contacts under the particle conservation model.

A. Results

We choose a band gap of 1 eV, as it is similar to the band gap of candidate HCSC absorber materials such as perovskites [43] and some III-V alloys [7]. While lower band gaps may result in a more efficient HCSC, the particle conservation model may not be valid, as Auger recombination becomes significant in low-band-gap semiconductors [5,6]. The goal of this study is to demonstrate the utilization of a QFLS in a thermionic barrier HCSC, which under the asymptotic limit of particle conservation does not directly correspond to a specific material system. Nonetheless, it is expected that the role of the QFLS is more important for high-band-gap absorbers.

Figure 6 shows the energy flows at the MPP for various barrier heights, where Eq. (9) was used to split the excess heat flow to the contact into its constituent reversible and irreversible components. Compared to the impact ionization model (Fig. 4), the cell efficiency is not as strongly affected by barrier height. For low barrier heights, the cell efficiency does not approach zero, as the high QFLS still provides power as in a conventional photovoltaic cell. For

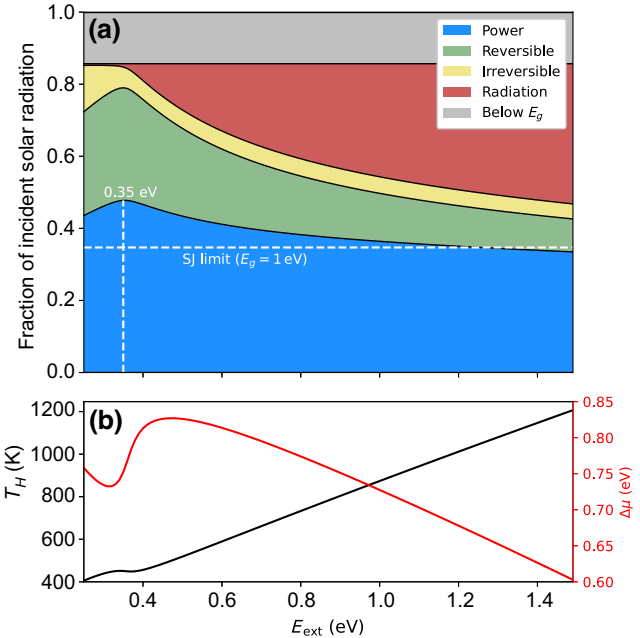


FIG. 6. (a) Breakdown of energy flows as a function of barrier height in a thermionic barrier HCSC under the particle conservation model, operating at MPP under 1000 Suns. The band gap is set to 1 eV, resulting in a constant below-band-gap transmission loss across all barrier heights. The dependence of the efficiency on the barrier height is not as significant as in the impact ionization model. The dashed line shows the single-junction efficiency for the same band gap and concentration. The HCSC surpasses this limit only for barriers below ~ 1.2 eV. (b) A QFLS allows for high voltages with low barriers and temperatures, and suppression of radiative recombination for high barriers and temperatures.

high barriers, even though the temperature is high, the light emission does not increase dramatically due to a lower QFLS, resulting in more energy being available for conduction than is the case in the impact ionization model. The resulting advantage is also clearly seen as a mostly constant, low irreversibility of the contact regardless of E_{ext} . The optimal operation for a 1-eV-band-gap absorber using particle conservation occurs at a significantly lower barrier height. It is less than 0.5 eV, compared to 1.6 eV for the impact ionization case. At this point the efficiency is boosted by the presence of the elevated carrier temperature but only slightly beyond the single-junction limit for the same band gap, as shown by the dashed line in Fig. 6(a).

Note that the maximum possible efficiency for a single-junction cell is achieved with a band gap of 1.16 eV, giving $\sim 1\%$ absolute higher efficiency than with $E_g = 1$ eV. Remarkably, the optimal barrier height corresponds to temperatures less than 200 K above the ambient, significantly lower compared to the temperature elevation of ~ 1000 K in the impact ionization model shown in Fig. 4. While high carrier temperatures and voltages are considered hallmarks

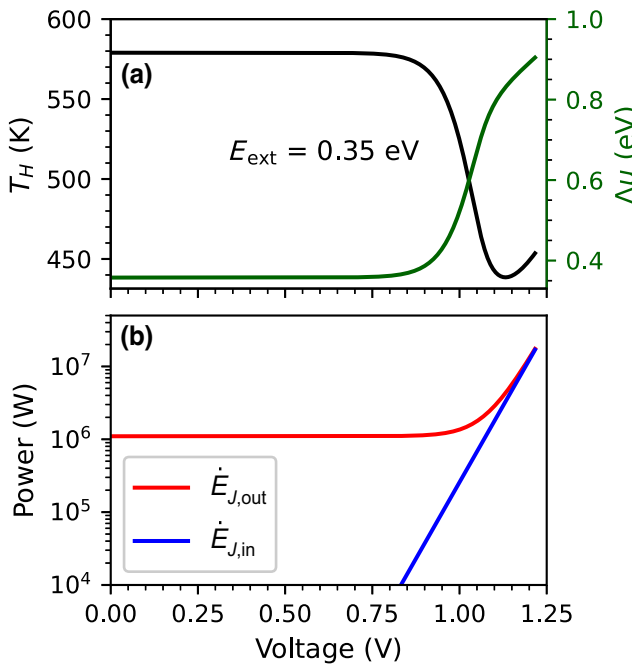


FIG. 7. Temperature-voltage characteristics of a thermionic barrier HCSC under the particle conservation model, operating under 1000 Suns with barrier height set to 0.35 eV. Similar to the impact ionization model, the temperature and QFLS are largely unchanged for small applied biases. However, a reduction in temperature is seen at high biases, in contrast to the trend in Fig. 5, compensated by an increase in the QFLS.

of HCSCs, they may not necessarily correspond to efficient operation, as highlighted by this result, obtained while neglecting electron cooling due to interactions with the lattice.

The temperature-voltage characteristics at the optimal barrier height are shown in Fig. 7. For high biases, the net current approaches zero and the emitted photon flux is high. This stems from a growing QFLS, but must be accompanied by a reduction in temperature to also satisfy energy conservation. This reduction in temperature is in contrast to the trend observed in the impact ionization model (Fig. 5).

VI. DISCUSSION

Any photovoltaic cell operates by creating a potential difference between the electron and hole contacts, such that power can be extracted from photogenerated current. In a conventional single-junction cell, this is achieved via a QFLS in the absorber which is in (quasi)equilibrium with the contacts. This QFLS is determined by the balance between generation and recombination. The highest achievable QFLS (and hence V_{oc}) is determined by the band gap.

In an HCSC (under the impact ionization model), the potential difference between the contacts is generated via a

temperature gradient between the absorber and contacts, which results from photon absorption by carriers in the absorber. By partially limiting carrier extraction via an energy-selective barrier, the elevated temperature can be maintained and converted to an electrochemical potential difference across the contacts.

An HCSC with a band gap can also additionally harness energy via a QFLS in the absorber (as shown in the particle conservation model results). The results in Fig. 6 show that the availability of this free energy can significantly lower the temperature required for optimal operation. Importantly, the thermal contribution to energy generation means that the V_{oc} limit of an HCSC is determined not by the band gap, but rather by the extraction energy.

The band gap and extraction energy therefore play analogous roles in single-junction and hot-carrier solar cells respectively: they determine the extent of loss mechanisms that significantly affect device operations and efficiency. In this work we have studied the tradeoff between energy flows that results in an optimal extraction energy for HCSCs, which we now compare to the equivalent compromise single-junction cells. For this comparison, we consider a zero-band-gap HCSC absorber (impact ionization model) with no phonon coupling and with nonideal contacts.

In a single-junction cell, a high-band-gap absorber can achieve a high V_{oc} , but the short-circuit current density J_{sc} is low since only a small portion of the incoming photons are absorbed. Analogously, the highest achievable V_{oc} by an HCSC is determined by the extraction energy E_{ext} . However, a high E_{ext} (unlike a high E_g) does not prevent absorption of photons; but it does limit current extraction, resulting in a large proportion of carriers losing the absorbed energy via radiative recombination.

A low band gap in a conventional cell results in a lower V_{oc} because the excess kinetic energy of the carriers is not exploited and is lost via phonons. In an ideal HCSC absorber, the excess kinetic energy is not lost to the lattice; however, low extraction energies result in a higher proportion of carriers losing excess energy as heat to the contacts. Since the current extracted and the excess heat dissipated to the contacts are inextricably linked to each other, the current-voltage compromise (similar to the one that exists in a single-junction cell) places a limit on heat flow minimization. The analogy described above is summarized in Table I. Note that considering an HCSC absorber with a band gap introduces transparency losses, and low band gaps are advantageous since the excess kinetic energy of the carriers can be utilized.

For the excess heat flow to be minimal regardless of the extraction energy (and the corresponding current and voltage), the extraction should be via an infinitesimally narrow window to minimally disturb the absorber carrier population. However, to extract a finite current from an infinitesimally narrow window, the contact conductivity

TABLE I. Comparison of loss mechanisms in single-junction (SJ) and hot-carrier solar cell (HCSC) devices.

Device type	Condition	Effect	Loss channel
SJ	High E_g	High V_{oc}	Transparency to photons
	Low E_g	Low J_{sc} High J_{sc}	Thermalization with lattice
		Low V_{oc}	
HCSC	High E_{ext}	High V_{oc}	Radiative emission
		High T_H Low J_{sc}	
	Low E_{ext}	High J_{sc}	Excess heat flow to contacts
		Low V_{oc} Low T_H	

needs to be infinite. This is the ideal ESC limit—in which the efficiency is independent of the extraction energy. This limit can asymptotically be approached by nonideal contacts as shown in Fig. 3.

Measuring carrier temperatures while varying parameters such as the extraction energy and applied electrical bias can therefore be a way of experimentally probing the loss mechanisms discussed above, reflecting the ideality of the contacts. Measurement of these relative temperature trends in devices could be a more straightforward and unambiguous way of proving HCSC operation, as reliably extracting absolute carrier temperatures from spectroscopy techniques such as photoluminescence can be challenging [44]. Since large barriers to carrier movement and/or extraction result in high carrier temperatures, high temperatures in spectroscopy of uncontacted materials could be a sign of inefficient carrier transport, suggesting the need for spatially resolved measurements for fully understanding absorber properties [45].

While this work does not consider the effect of carrier cooling, which may result from electron-phonon interactions, it has been shown that, under the impact ionization model, heat exchange with the lattice has a severe impact on HCSC efficiency and barrier optimization [24]. The optimal barrier height is lower for cooler carrier distributions, and the efficiency is completely diminished if carriers are cooled to the ambient temperature. On the other hand, due to lower operating temperatures in the particle conservation model, the power loss to the lattice is expected to be lower. Even when carriers have completely cooled to the ambient temperature, the efficiency does not go to zero due to the QFLS. This suggests that semiconductor HCSC absorbers with low impact-Auger rates may be more robust against energy losses associated with carrier cooling.

In conclusion, we have demonstrated the importance of heat flows in hot-carrier solar cells and how they determine optimal contact parameters. We have shown the characteristics of an HCSC with a thermionic barrier contact using both the impact ionization and particle conservation models. By defining a measure of the irreversibility of the carrier extraction, we have shown how highly conductive QDs with Gaussian transmission functions would minimize the irreversible component of the heat flow and enable high efficiencies.

- [1] R. T. Ross and A. J. Nozik, Efficiency of hot-carrier solar energy converters, *J. Appl. Phys.* **53**, 3813 (1982).
- [2] P. Würfel, Solar energy conversion with hot electrons from impact ionisation, *Solar Energy Mater. Solar Cells* **46**, 43 (1997).
- [3] W. Shockley and H. J. Queisser, Detailed balance limit of efficiency of p-n junction solar cells, *J. Appl. Phys.* **32**, 510 (1961).
- [4] Y. Takeda, T. Motohiro, D. König, P. Aliberti, Y. Feng, S. Shrestha, and G. Conibeer, Practical factors lowering conversion efficiency of hot carrier solar cells, *Appl. Phys. Express* **3**, 104301 (2010).
- [5] P. Würfel, A. S. Brown, T. E. Humphrey, and M. A. Green, Particle conservation in the hot-carrier solar cell, *Prog. Photovolt.: Res. Appl.* **13**, 277 (2005).
- [6] Y. Takeda, T. Ito, R. Suzuki, T. Motohiro, S. Shrestha, and G. Conibeer, Impact ionization and Auger recombination at high carrier temperature, *Solar Energy Materials and Solar Cells 17th International Photovoltaic Science and Engineering Conference* **93**, 797 (2009).
- [7] L. C. Hirst, R. J. Walters, M. F. Führer, and N. J. Ekins-Daukes, Experimental demonstration of hot-carrier photocurrent in an InGaAs quantum well solar cell, *Appl. Phys. Lett.* **104**, 231115 (2014).
- [8] S. Limpert, A. Burke, I.-J. Chen, N. Anttu, S. Lehmann, S. Fahlvik, S. Bremner, G. Conibeer, C. Thelander, M.-E. Pistol, and H. Linke, Single-nanowire, low-bandgap hot carrier solar cells with tunable open-circuit voltage, *Nanotechnology* **28**, 434001 (2017).
- [9] J. A. R. Dimmock, M. Kauer, J. Wu, H. Liu, P. N. Stavrinou, and N. J. Ekins-Daukes, A metallic hot-carrier photovoltaic device, *Semicond. Sci. Technol.* **34**, 064001 (2019).
- [10] J. A. R. Dimmock, S. Day, M. Kauer, K. Smith, and J. Heffernan, Demonstration of a hot-carrier photovoltaic cell, *Prog. Photovolt.: Res. Appl.* **22**, 151 (2014).
- [11] K. J. Williams, C. A. Nelson, X. Yan, L.-S. Li, and X. Zhu, Hot electron injection from graphene quantum dots to TiO₂, *ACS Nano* **7**, 1388 (2013).
- [12] S. Kahmann and M. A. Loi, Hot carrier solar cells and the potential of perovskites for breaking the Shockley–Queisser limit, *J. Mater. Chem. C* **7**, 2471 (2019).
- [13] J. Yang, X. Wen, H. Xia, R. Sheng, Q. Ma, J. Kim, P. Tapping, T. Harada, T. W. Kee, F. Huang, Y.-B. Cheng, M. Green, A. Ho-Baillie, S. Huang, S. Shrestha, R. Patterson, and G. Conibeer, Acoustic-optical phonon up-conversion and hot-phonon bottleneck in lead-halide perovskites, *Nat. Commun.* **8**, 1 (2017).

- [14] R. Clady, M. J. Y. Tayebjee, P. Aliberti, D. König, N. J. Ekins-Daukes, G. J. Conibeer, T. W. Schmidt, and M. A. Green, Interplay between the hot phonon effect and inter-valley scattering on the cooling rate of hot carriers in GaAs and InP, *Prog. Photovolt.: Res. Appl.* **20**, 82 (2012).
- [15] A. A. Balandin, Nanophononics: Phonon engineering in nanostructures and nanodevices, *J. Nanosci. Nanotechnol.* **5**, 1015 (2005).
- [16] E. M. Weig, R. H. Blick, T. Brandes, J. Kirschbaum, W. Wegscheider, M. Bichler, and J. P. Kotthaus, Single-Electron-Phonon Interaction in a Suspended Quantum Dot Phonon Cavity, *Phys. Rev. Lett.* **92**, 046804 (2004).
- [17] P. Roulleau, S. Baer, T. Choi, F. Molitor, J. Güttinger, T. Müller, S. Dröscher, K. Ensslin, and T. Ihn, Coherent electron–phonon coupling in tailored quantum systems, *Nat. Commun.* **2**, 239 (2011), number 1.
- [18] G. J. Conibeer, C. W. Jiang, D. König, S. Shrestha, T. Walsh, and M. A. Green, Selective energy contacts for hot carrier solar cells, *Thin Solid Films Proceedings on Advanced Materials and Concepts for Photovoltaics EMRS 2007 Conference, Strasbourg, France*, **516**, 6968 (2008).
- [19] I. Konovalov, V. Emelianov, and R. Linke, Hot carrier solar cell with semi infinite energy filtering, *Solar Energy* **111**, 1 (2015).
- [20] T. E. Humphrey, M. F. O'Dwyer, and H. Linke, Power optimization in thermionic devices, *J. Phys. D: Appl. Phys.* **38**, 2051 (2005).
- [21] M. F. O'Dwyer, T. E. Humphrey, R. A. Lewis, and C. Zhang, Electronic and thermal transport in hot carrier solar cells with low-dimensional contacts, *Microelectronics Journal The Sixth International Conference on Low Dimensional Structures and Devices*, **39**, 656 (2008).
- [22] A. Le Bris and J.-F. Guillemoles, Hot carrier solar cells: Achievable efficiency accounting for heat losses in the absorber and through contacts, *Appl. Phys. Lett.* **97**, 113506 (2010).
- [23] Y. Takeda, Hot-carrier solar cells and improved types using wide-bandgap energy-selective contacts, *Prog. Photovolt.: Res. Appl.* **30**, 65 (2022).
- [24] I. Konovalov and B. Ploss, Modeling of hot carrier solar cell with semi-infinite energy filtering, *Solar Energy* **185**, 59 (2019).
- [25] Y. Takeda, in *Quantum Dot Solar Cells*, Lecture Notes in Nanoscale Science and Technology, edited by J. Wu and Z. M. Wang (Springer, New York, NY, 2014), p. 187.
- [26] S. Limpert, S. Bremner, and H. Linke, Reversible electron–hole separation in a hot carrier solar cell, *New J. Phys.* **17**, 095004 (2015).
- [27] A. Pusch, M. Dubajic, M. P. Nielsen, G. J. Conibeer, S. P. Bremner, and N. J. Ekins-Daukes, Optoelectronic reciprocity in hot carrier solar cells with ideal energy selective contacts, *Prog. Photovolt.: Res. Appl.* **29**, 433 (2021).
- [28] N. Harada and S. Kuroda, Lifetime of resonant state in a resonant tunneling system, *Jpn. J. Appl. Phys.* **25**, L871 (1986).
- [29] Y. Liao, P. Zhang, S. Bremner, S. Shrestha, S. Huang, and G. Conibeer, Resonant tunneling through monolayer Si colloidal quantum dots and Ge nanocrystals, *Adv. Funct. Mater.* **27**, 1605348 (2017).
- [30] T. Bryllert, M. Borgstrom, T. Sass, B. Gustafson, L. Landin, L.-E. Wernersson, W. Seifert, and L. Samuelson, Designed emitter states in resonant tunneling through quantum dots, *Appl. Phys. Lett.* **80**, 2681 (2002).
- [31] A. A. Grinberg, Thermionic emission in heterosystems with different effective electronic masses, *Phys. Rev. B* **33**, 7256 (1986).
- [32] C. R. Crowell, Richardson constant and tunneling effective mass for thermionic and thermionic-field emission in Schottky barrier diodes, *Solid State Electron.* **12**, 55 (1969).
- [33] D. Sinha and J. U. Lee, Ideal graphene/silicon Schottky junction diodes, *Nano Lett.* **14**, 4660 (2014).
- [34] S. Bahl, M. Leary, and J. del Alamo, Mesa-sidewall gate leakage in InAlAs/InGaAs heterostructure field-effect transistors, *IEEE Trans. Electron. Devices* **39**, 2037 (1992).
- [35] L. S. Yu, Q. Z. Liu, Q. J. Xing, D. J. Qiao, S. S. Lau, and J. Redwing, The role of the tunneling component in the current–voltage characteristics of metal-GaN Schottky diodes, *J. Appl. Phys.* **84**, 2099 (1998).
- [36] A. A. M. Farag, F. S. Terra, G. M. Mahmoud, and A. M. Mansour, Study of Gaussian distribution of inhomogeneous barrier height for n-InSb/p-GaAs heterojunction prepared by flash evaporation, *J. Alloys Compd.* **481**, 427 (2009).
- [37] Y. Feng, P. Aliberti, B. P. Veetttil, R. Patterson, S. Shrestha, M. A. Green, and G. Conibeer, Non-ideal energy selective contacts and their effect on the performance of a hot carrier solar cell with an indium nitride absorber, *Appl. Phys. Lett.* **100**, 053502 (2012).
- [38] S. Mukherjee, S. Mukherjee, A. Pradhan, T. Maitra, S. Sengupta, S. Chakrabarti, A. Nayak, and S. Bhunia, Carrier transport and recombination dynamics of InAs/GaAs sub-monolayer quantum dot near infrared photodetector, *J. Phys. D: Appl. Phys.* **52**, 505107 (2019).
- [39] N. Vukmirović, Z. Ikonić, I. Savić, D. Indjin, and P. Harrison, A microscopic model of electron transport in quantum dot infrared photodetectors, *J. Appl. Phys.* **100**, 074502 (2006).
- [40] D. Pan, E. Towe, and S. Kennerly, A five-period normal-incidence (In,Ga)As/GaAs quantum-dot infrared photodetector, *Appl. Phys. Lett.* **75**, 2719 (1999).
- [41] K. H. Schmidt, M. Versen, U. Kunze, D. Reuter, and A. D. Wieck, Electron transport through a single InAs quantum dot, *Phys. Rev. B* **62**, 15879 (2000).
- [42] I. Hapke-Wurst, U. Zeitler, U. F. Keyser, R. J. Haug, K. Pierz, and Z. Ma, Tuning the onset voltage of resonant tunneling through InAs quantum dots by growth parameters, *Appl. Phys. Lett.* **82**, 1209 (2003).
- [43] M. Li, J. Fu, Q. Xu, and T. C. Sum, Slow hot-carrier cooling in halide perovskites: Prospects for hot-carrier solar cells, *Adv. Mater.* **31**, 1802486 (2019).
- [44] F. Gibelli, L. Lombez, and J.-F. Guillemoles, Accurate radiation temperature and chemical potential from quantitative photoluminescence analysis of hot carrier populations, *J. Phys.: Condensed Matter* **29**, 06LT02 (2016).
- [45] A. Block, M. Liebel, R. Yu, M. Spector, Y. Sivan, F. J. G. d. Abajo, and N. F. v. Hulst, Tracking ultrafast hot-electron diffusion in space and time by ultrafast thermomodulation microscopy, *Sci. Adv.* **5**, eaav8965 (2019).